A THREE-DIMENSIONAL WAVELET ANALYSIS OF SUBSTRUCTURE IN THE COMA CLUSTER: STATISTICS AND MORPHOLOGY

M. GAMBERA AND A. PAGLIARO

Istituto di Astronomia, Università di Catania, Città Universitaria, Viale Andrea Doria 6, I-95125 Catania, Italy

AND

V. ANTONUCCIO-DELOGU[1] AND U. BECCIANI

Osservatorio Astrofisico di Catania, Città Universitaria, Viale Andrea Doria 6, I-95125 Catania, Italy

Received 1997 January 27; accepted 1997 May 22

ABSTRACT

Evidence of clustering within the Coma Cluster is found by means of a multiscale analysis of the combined angular-redshift distribution. We have compiled a catalog of 798 galaxy redshifts from published surveys of the region of the Coma Cluster. We examine the presence of substructure and of voids at different scales ranging from ~ 1 to ~ 16 h^{-1} Mpc, using subsamples of the catalog ranging from $cz = 3000$ km s^{-1} to $cz = 28,000$ km s^{-1}. Our substructure detection method is based on the wavelet transform and on segmentation analysis. The wavelet transform allows us to find structures at different scales, and the segmentation method allows a quantitative statistical and morphological analysis of the sample. From the whole catalog, we select a subset of 320 galaxies, with redshifts between $cz = 5858$ km s^{-1} and $cz = 8168$ km s^{-1}, which we identify as belonging to the central region of Coma and upon which we have performed a deeper analysis, on scales ranging from 180 h^{-1} kpc to 1.44 h^{-1} Mpc. Our results are expressed in terms of the number of structures or voids and their sphericity for different values of the threshold detection and at all the scales investigated. According to our analysis, there is strong evidence of multiple hierarchical substructure, on scales ranging from a few hundreds of kiloparsecs to about 4 h^{-1} Mpc. The morphology of these substructures is rather spherical. On a scale of 720 h^{-1} kpc we find two main subclusters that have been found before, but our wavelet analysis shows even more substructures, whose redshift position is approximately marked by the following bright galaxies: NGC 4934 and 4840, NGC 4889, NGC 4898 and 4864, NGC 4874 and 4839, NGC 4927, and NGC 4875.

Subject headings: galaxies: clusters: individual (Coma) — methods: statistical — surveys

1. INTRODUCTION

The Coma Cluster (number 1656 in the Abell 1958 catalog) has been perhaps the most studied galaxy cluster since 1933, when Zwicky calculated its mass (Zwicky 1933). It has long been quoted as the paradigmatic example of a roughly spherical, relaxed cluster (Sarazin 1986). Previous papers (e.g., Fitchett & Webster 1987; Mellier et al. 1988; Baier, Fritze, & Tiersch 1990; Briel, Henry, & Böhringer 1992; White, Briel, & Henry 1993; Colless & Dunn 1996, hereafter CD96; Biviano et al. 1996) have suggested that this cluster may have a complex structure. The X-ray images obtained with *ROSAT* suggest the presence of clumps of emission associated with substructures (Briel et al. 1992; White et al. 1993). However, previous analyses were performed only on two-dimensional slices of the cluster. In this paper, we take up the issue of substructure in this cluster from yet another point of view, namely, by trying to make use of redshift information.

Our aim is to find substructure or voids at different scales through a three-dimensional analysis of the cluster, identify them, and make a morphological analysis. As will become evident, our wavelet analysis detects substructure that is not visible in two-dimensional images, either optical or X-ray.

The plan of the paper is as follows: In § 2, we discuss the selection criteria that we have adopted to assemble our catalog. In §§ 3 and 4, we discuss the method of analysis based on wavelet transform and segmentation. In § 5, we report our results concerning the number and morphology of substructures, and in § 6 we do the same for the central region of the cluster. In § 7, we make some cautionary remarks concerning the statistical and physical significance of our analysis, and finally, in § 8 we report our conclusions.

2. DATA

A large body of data on the Coma Cluster is available in the literature. Our catalog has been collected by exploiting data from different redshift surveys. In total, we have selected 798 redshifts for galaxies lying in the range

$$\text{R.A.} = 10^h42^m00^s \text{ to } 15^h28^m00^s,$$

$$\text{decl.} = +26°30'00'' \text{ to } +29°55'00'' \quad (1)$$

(B1950.0; hereafter all coordinates are referred to 1950.0). The redshifts for 243 galaxies have been kindly provided to us in electronic form by J. Colless and come from the new redshift survey by CD96. The mean redshift uncertainty is about 50 km s^{-1}, and the uncertainty in the positions is less than 1″. Another sample of 305 redshifts was taken from Biviano et al. (1996), 225 of which are new measurements made at the Canada-France-Hawaii Telescope; the mean uncertainty is about 100 km s^{-1}. The positions in this catalog are known with a mean error of about 2″. Another 320 redshifts have been taken from the catalog of 379 galaxies by Karachentsev & Kopylov (1990). The mean uncertainty in their measurements is 100 km s^{-1}, while the mean error in the positions is $\pm 3''$. Finally, 46 redshifts have been

[1] Also Theoretical Astrophysics Center, Copenhagen, Denmark.

TABLE 1

CATALOGS USED IN OUR ANALYSIS

Catalog	Number of Galaxies	$\langle cz \rangle$	σ_{cz}	$(cz)_{min}$	$(cz)_{max}$
C_{ext}	690	10541 ± 115	6056 ± 98	3000	28000
C	485	7013 ± 100	1155 ± 80	4000	10000
C_{cen}	320	7034 ± 80	597 ± 70	5858	8168

NOTE.—Redshifts are in km s^{-1}.

taken from the NASA/IPAC Extragalactic Database. This latter set of data is heterogeneous; however, the quoted mean uncertainty is less than ~ 120 km s^{-1}, while the positions are known with a mean error of about 6″.

The total number of galaxies so collected is 914, but some objects are common to the three data sets. We have considered a galaxy to be in common when its position in a given data set is inside the mean error in the coordinate determination of a different set. So, if several redshift measurements were available for the same galaxy, we have included only the most accurate. The completeness of our heterogeneous catalog is about 85% at $m_B = 18$. This value has been calculated from a weighted mean of the values for the different databases used in our compilation.

To summarize, we have a heterogeneous sample of redshifts for 798 galaxies with 1000 km s$^{-1} \leq cz \leq 115,000$ km s^{-1}. As coordinates for the cluster's photometric center, we chose the value quoted by Godwin, Metcalfe, & Peach (1983): R.A. $= 12^h57^m.3$ and decl. $= +28°14'.4$. The uncertainty on the redshift measurements is about 100 km s^{-1}, and the maximum error on the positions is less than 3″. From this catalog we extract three different subsamples, as shown in Table 1. The line-of-sight distribution for the galaxies of our subsample with 3000 km s$^{-1} < cz < 28,000$ km s^{-1} is shown in Figure 1a. Hereafter we call this region C_{ext}.

The number of galaxies inside this region is 690. Already this histogram seems to suggest the presence of two main peaks in the redshift distribution.

Subsample C_{ext} has a mean redshift $\langle cz \rangle = 10,541 \pm 115$ km s^{-1} and a standard deviation $\sigma_{cz} = 6056 \pm 98$ km s^{-1}. The galaxies of the first peak have redshifts 4000 km s$^{-1} \leq cz \leq 10,000$ km s^{-1}, the mean redshift and the standard deviation being respectively $\langle cz \rangle = 7013 \pm 100$ km s^{-1} and $\sigma_{cz} = 1155 \pm 80$ km s^{-1}. The line-of-sight velocity dispersion for the galaxies of the first peak is $\sigma_v = 1128 \pm 78$ km s^{-1}. The galaxies of the second peak have redshifts 16,100 km s$^{-1} \leq cz \leq 24,600$ km s^{-1}, the mean redshift and standard deviation being respectively $\langle cz \rangle = 19,918 \pm 100$ km s^{-1} and $\sigma_{cz} = 3745 \pm 80$ km s^{-1}. In Figure 1b, only those galaxies inside the first peak are considered and the line-of-sight distribution is shown. Hereafter we call this region C. The number of galaxies inside C is 485. From Figure 1b, we note that the distribution of Coma galaxies in the redshift field shows the presence of some peaks, and this also may suggest the existence of multiple substructure.

We have transformed the angular distances from the photometric center to a linear one by assuming a distance from the center of the cluster equal to the mean value of the redshift divided by H_0. Finally, to make our linear coordi-
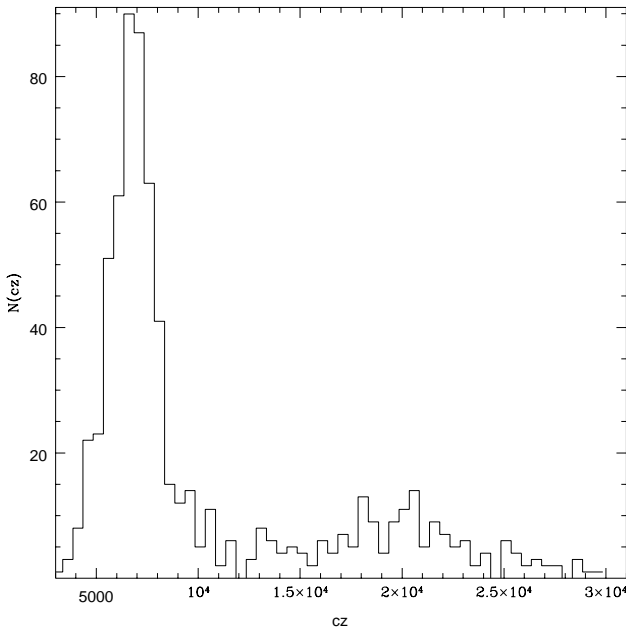

FIG. 1a

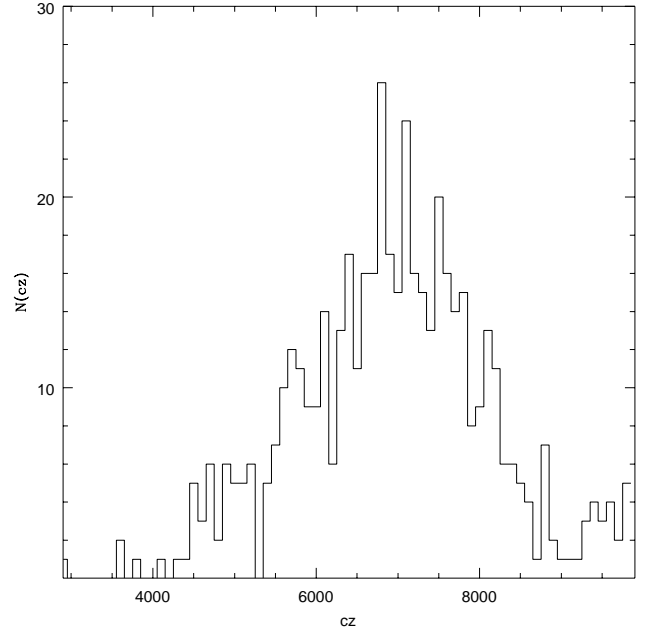
FIG. 1b

FIG. 1.—(a) Histogram of the galaxy distribution, with redshifts 3000 km s$^{-1} \leq cz \leq 28,000$ km s^{-1} inside C_{ext}, according to our catalog. The step size is 500 km s^{-1}. (b) Histogram of the galaxy distribution, with redshifts 4000 km s$^{-1} \leq cz \leq 10,000$ inside C, according to our catalog. The step size is 100 km s^{-1}.

nates independent of the value of H_0, we renormalize them by dividing by σ_{cz}.

3. METHOD OF ANALYSIS: WAVELET TRANSFORM AND SEGMENTATION

3.1. *Wavelet Transform*

Our method of structure detection is based on the wavelet transform evaluated at several scales and on a segmentation analysis; the method is similar to that developed by Lega (1994, hereafter L94; part of this Ph.D. thesis may be found in Lega et al. 1995, 1996).

A detailed description of the implementation of the algorithms is beyond the purpose of this paper. A parallel version for a Connection Machine CM-200 has been developed by Lega (L94), and a new parallel virtual machine version will be described in Pagliaro & Becciani (1997). Although the method that we implement is three-dimensional, for simplicity we describe here the one-dimensional version; generalization to the three-dimensional case is straightforward.

For a one-dimensional function $f(x)$, the wavelet transform is a linear operator that can be written as

$$w(s, t) = \langle f \mid \psi \rangle$$
$$= s^{-1/2} \int_{-\infty}^{+\infty} f(x)\psi^*\left(\frac{x-t}{s}\right)dx \, , \quad (2)$$

where s (> 0) is the scale on which the analysis is performed, $t \in \mathbf{R}$ is the spatial translation parameter, and ψ is the Grossmann-Morlet (1984, 1987) analyzing wavelet function

$$\psi_{(s,t)}(x) = s^{-1/2}\psi\left(\frac{x-t}{s}\right) , \quad (3)$$

which is spatially centered around t and has scale s. The wavelet function $\psi_{(1,0)}(x)$ is called the *mother wavelet*. It generates the other wavelet functions $\psi_{(s,t)}(x)$, $s > 1$. We follow L94 in the choice of the mother wavelet:

$$\psi_{(s,t)}(x) = \phi(x) - \tfrac{1}{2}\phi(x/2) , \quad (4)$$

where ϕ is the cubic-centered B-spline function defined by

$$\phi(x) = \tfrac{1}{12}(\mid x - 2\mid^3 - 4\mid x - 1\mid^3$$
$$+ 6\mid x\mid^3 - 4\mid x + 1\mid^3 + \mid x + 2\mid^3) . \quad (5)$$

Although our data distribution is highly anisotropic, we prefer to use an isotropic wavelet function and to perform a scale transformation along the z (redshift) axis.

With these choices, the wavelet coefficients at different scales can be calculated by the *à trous* algorithm, as described by L94 (p. 100), which is extremely fast and requires the set of scales to be powers of 2: $s = 2^r$.

The scale s in this kind of analysis may be considered the resolution. In other words, if we perform a calculation on a scale s_0, we expect the wavelet transform to be sensitive to structures with typical size of about s_0 and to find those structures.

3.2. *Choice of Threshold*

The thresholding is made on the wavelet coefficient histogram. For a flat background, the wavelet transform yields zero coefficients. The existence of structures at a given scale yields wavelet coefficients with large positive values. Obviously, a random distribution may result in coefficients that

are different even if there is no structure, as a result of statistical fluctuations. Moreover, the statistical behavior of the wavelet coefficient is complex because of the existence of correlations among nearby background structures, which manifest as correlations among nearby pixels.

In order to single out significant structures, we have to fix a thresholding criterion and level. We choose the threshold using a classical decision rule. We calculate the wavelet coefficients $w_{ran}(s)$ for each scale of our analysis, for 10 random distributions in the same region of space as our data and on the same grid. Then we calculate the probability $P[w(s) \leq w_{ran}(s)]$ and choose the value $w_{thres}(s)$ so that

$$P[w_{thres}(s) \leq w_{ran}(s)] \leq \epsilon \, . \quad (6)$$

Our threshold on the scale s is the value $v_{thres} = w_{thres}(s)$. Our choice for the value of ϵ is

$$\epsilon = 0.001 \, , \quad (7)$$

which ensures a 99.9% confidence level in the structure detection. However, for the sake of completeness, we perform our analysis for several values of the threshold, calculated in terms of the standard deviation in the wavelet coefficient distribution of our data.

3.3. *Structure Numbering through Segmentation*

The second step in our analysis is the determination of connected pixels over a fixed threshold (*segmentation*; Rosenfeld 1969), the numbering of the selected structures, and their morphological analysis.

The segmentation and numbering consist of the analysis of the matrix of wavelet coefficients; all the pixels associated with a wavelet coefficient greater than the selected threshold are labeled with an integer. All other pixels' labels are set to zero. Then the same label is associated with all the pixels connected in a single structure, in a sequential way. So, the first structure individuated has the label "1," and so on. Then, for each structure, we calculate volume and surface and from them a morphological parameter.

A detailed description of the algorithm is beyond the scope of this paper. However, it can be described in brief as follows: *Step 1.*—All pixels with $w \geq v_{thres}$ are labeled. *Step 2.*—The same label is associated with those pixels labeled and connected. This is done in a sequential way; the first structure detected has the label "1," the Nth one has the label "N." This requires a renumbering of most pixels. *Step 3.*—The volume and surface of each structure singled out are calculated.

3.4. *Morphological Parameter*

In order to perform a morphological analysis, we have to introduce a morphological parameter that quantifies the sphericity of the structures. We choose the parameter

$$L(s) = K(s)V^2/S^3 \, , \quad (8)$$

where V is the volume and S is the surface, as in L94, and $K(s)$ is a parameter that depends on the scale of analysis. We want $L(s)$ to have the following behavior: zero for very filamentary structures and 1 for spherical ones. This may be achieved by setting $K = 36\pi$, but only for those scales not affected by the granular nature of the analysis. We choose the value 36π only for the scale $s = 2^r$ pixels with $r \geq 2$. For the smallest scales the constant 36π is not adequate, since we are close to the grid resolution and the geometry of the substructures cannot be spherical. So, since we want to con-
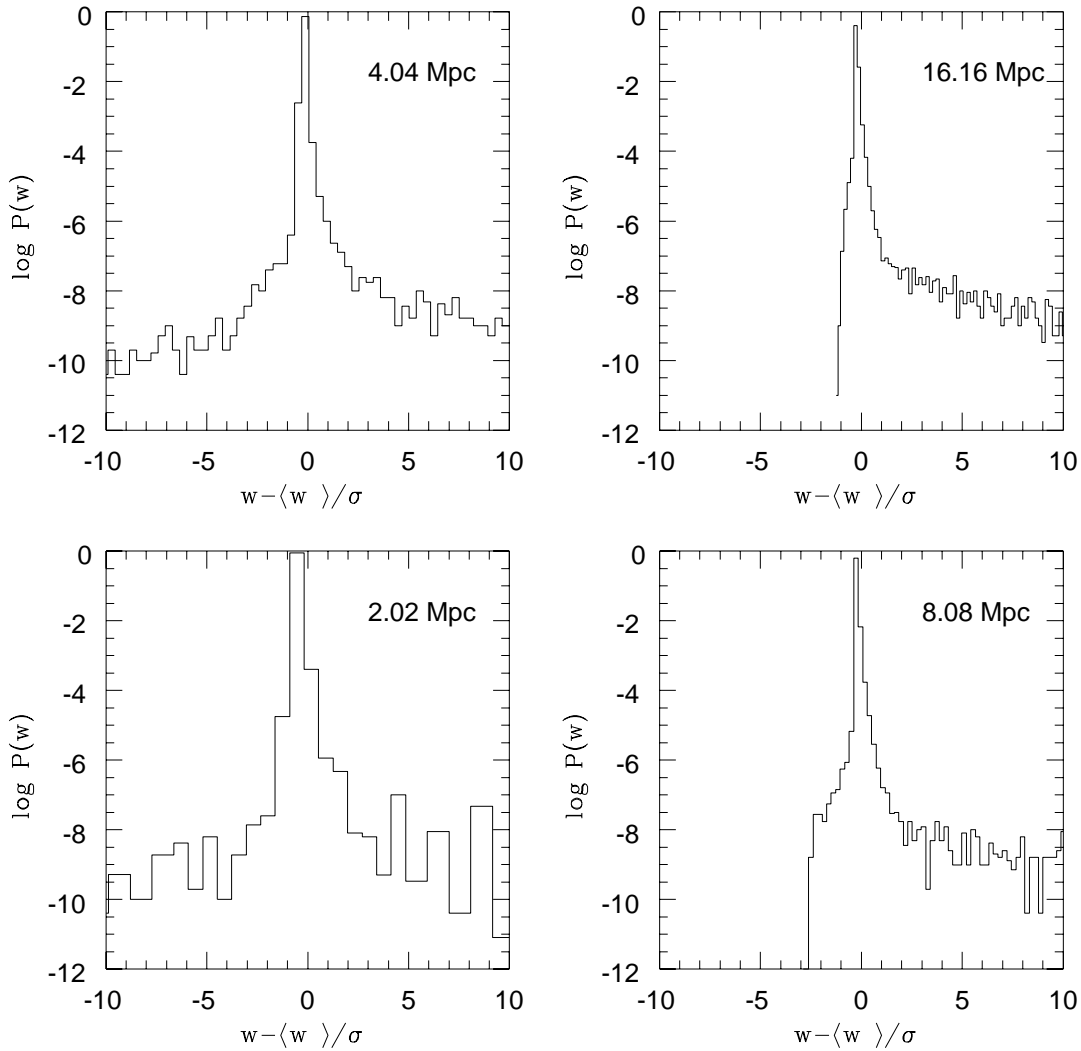
FIG. 2.—Histograms of the wavelet coefficients on the four scales selected for C_{ext}

sider as spherical a 1 pixel structure, we adopt the values

$$K(2^r) = \begin{cases} 216 \, , & \text{if } r = 0 \text{ or } 1, \\ 36\pi \, , & \text{otherwise} \, . \end{cases} \quad (9)$$

Then, for every detection threshold, we calculate the values

$$\langle L(s) \rangle = \sum_{i=1}^{N_{obj}} \frac{L(s)}{N_{obj}} \, , \quad (10)$$

where N_{obj} is the number of objects detected at scale s.

4. VOID DETECTION METHOD

The void detection method is analogous to the structure detection method, as far as "greater than" is replaced by

TABLE 2

RESULTS FOR C_{ext}

Scale (h^{-1} Mpc)	99.9%	3 σ	4 σ	5 σ	Voids
A. Number of Structures					
2.02	60	63	55	64	65
4.04	15	4	4	4	2
8.08	2	1	1	1	4
16.16	2	1	2	2	0
B. Morphology					
2.02	0.93	0.90	0.91	0.91	0.84
4.04	0.52	0.40	0.45	0.27	0.13
8.08	0.30	0.27	0.27	0.31	0.42
16.16	0.17	0.17	0.30	0.31	...

NOTES.—Number of structures and mean morphological parameter $\langle L \rangle$ at different scales and over different thresholds for the catalog C_{ext}.

TABLE 3

RESULTS FOR C

Scale (h^{-1} Mpc)	99.9%	3 σ	4 σ	5 σ	Voids
A. Number of Structures					
0.47	54	205	200	75	40
0.94	21	42	35	25	12
1.88	3	3	2	3	0
3.76	2	1	1	2	0
B. Morphology					
0.47	0.95	0.88	0.89	0.89	0.94
0.94	0.85	0.64	0.62	0.58	0.60
1.88	0.19	0.42	0.32	0.60	...
3.76	0.16	0.10	0.13	0.12	...

NOTE.—Same as Table 2, but for catalog C.
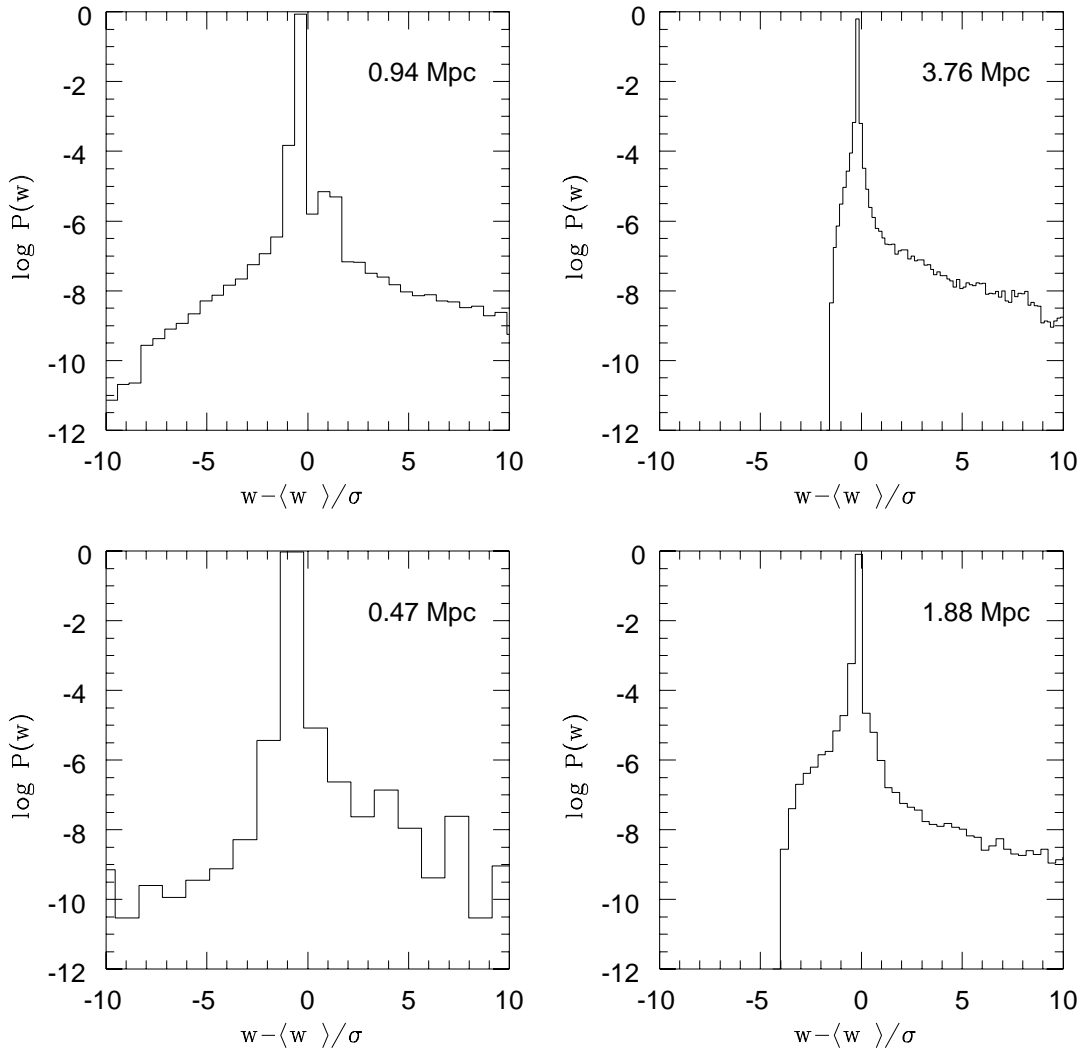
FIG. 3.—Same as Fig. 2, but for catalog C

"less than." The void thresholding is also made on the wavelet coefficient histogram. The presence of voids at a given scale yields wavelet coefficients with large negative values.

Our choice for the threshold is the same as in § 3.2. We calculate the wavelet coefficients $w_{ran}(s)$ for each scale of our analysis, for 10 random distributions in the same region of space as our data. Then we calculate the probability $P[w(s) \geq w_{ran}(s)]$ and choose the value $w_{voids}(s)$ so that

$$P[w_{voids}(s) \geq w_{ran}(s)] \leq \epsilon \qquad (11)$$

with $\epsilon = 0.001$, which ensures a 99.9% confidence level in the void detection. Our threshold is the value $v_{voids} = w_{voids}(s)$. Obviously, in the segmentation algorithm for the void detection the labeled pixels are those with wavelet coefficients $w \leq v_{voids}$.

The determination of the voids' morphological parameter values is analogous to the determination of structures' morphological parameter values, described in § 3.4.

5. SUBSTRUCTURE AND VOID DETECTION IN THE COMA CLUSTER

We examine two catalogs. The first is C_{ext}, made of 690 galaxies, as previously stated, with redshifts between

$cz = 3000$ km s^{-1} and $cz = 28,000$ km s^{-1}. Our grid ensures a resolution of about 2 h^{-1} Mpc on each of the three axes. We examine four different scales, 2.02, 4.04, 8.08, and 16.16 h^{-1} Mpc, for four different values of the threshold: the 99.9% confidence level as described in § 3, and then 3 σ, 4 σ, and 5 σ, where σ is the standard deviation in the wavelet coefficient distribution for the selected scale. The second catalog investigated is C. It is made of 485 galaxies with redshifts between $cz = 4000$ km s^{-1} and $cz = 10,000$ km s^{-1}. Our analysis grid ensures a resolution of about 470 h^{-1} kpc on each of the three axes. We examine four different scales, 0.47, 0.94, 1.88, and 3.76 h^{-1} Mpc, for the same four values of the threshold as above. We show the wavelet coefficient distributions on the four scales for the two catalogs in Figures 2 and 3. We plot the value $(w - \langle w \rangle)/\sigma$, where w is the wavelet coefficient's value and $\langle w \rangle$ and σ are respectively the mean and the standard deviation in the wavelet coefficient distribution, versus $\log P(w)$, where $P(w)$ is the probability associated with the wavelet coefficient w. The curves are slightly asymmetric on all scales, with a small skew toward positive values of the coefficients, indicating the presence of substructure. Our results are expressed in terms of the number of structures at the selected scales (see Tables 2 and 3). Considering the 99.9% confidence level as a significance level for the structure detection, we have over-

whelming evidence of substructure inside the Coma Cluster on scales from 0.47 to 4.04 h^{-1} Mpc. On smaller scales the evidence is certainly less, as one can also see from the fact that on these scales the wavelet coefficient histograms are more symmetric.

In Tables 2 and 3, we show the morphological parameter $\langle L \rangle$. For catalog C, our substructures are rather spherical on the first two scales. The value of $\langle L \rangle$ is lowered to 0.2 on the scale 1.88 h^{-1} Mpc, indicating a much more filamentary morphology for those structures singled out at this resolution. The substructure of C_{ext}, singled out with a greater resolution, shows a spherical morphology until the scale of 2.02 h^{-1} Mpc; more elongated shapes are found at the larger scales. In both cases, the diminution of $\langle L \rangle$ and of the number of structures as a function of scale indicates a hierarchical distribution.

6. THE CENTRAL REGION OF COMA

6.1. Substructures

We consider a galaxy to belong to the central region of Coma if its redshift is within ± 1 σ of $\langle cz \rangle = 7013$ km s^{-1}, where $\langle cz \rangle$ and σ are respectively the mean and the standard deviation in the redshift distribution calculated for the 485 galaxies considered in § 5. Our catalog C_{cen} is made of

320 galaxies, with redshifts between $cz = 5858$ km s^{-1} and $cz = 8168$ km s^{-1}. The mean redshift is $\langle cz \rangle = 7034 \pm 80$ km s^{-1}, and the standard deviation is $\sigma_{cz} = 597 \pm 70$ km s^{-1}. Our grid ensures a resolution of about 180 h^{-1} kpc on each of the three axes. We examine four different scales, 180, 360, 720, and 1440 h^{-1} kpc, for the usual values of the threshold ranging from 3 σ to 5 σ plus the 99.9% confidence level threshold, where σ is the standard deviation in the wavelet coefficient distribution for the selected scale. We show the wavelet coefficient distributions on the four scales in Figure 4. These are slightly asymmetric too, with the usual small skew toward positive values, indicating the presence of substructure inside the central region of the cluster as well. Our results are expressed in terms of the number of structures at the selected scales. Considering the 99.9% confidence level threshold as significance level for the structure detection, we have overwhelming evidence of substructure inside the central region of the Coma Cluster on the first three scales investigated, 180, 360, and 720 h^{-1} kpc (see Table 4A). The morphological parameter is shown in Table 4B. Our substructures are rather spherical on all scales but the last, with a value of about 0.5 for the morphological parameter, showing that the shape becomes more elongated on a scale of typical size 720 h^{-1} kpc inside the central region.
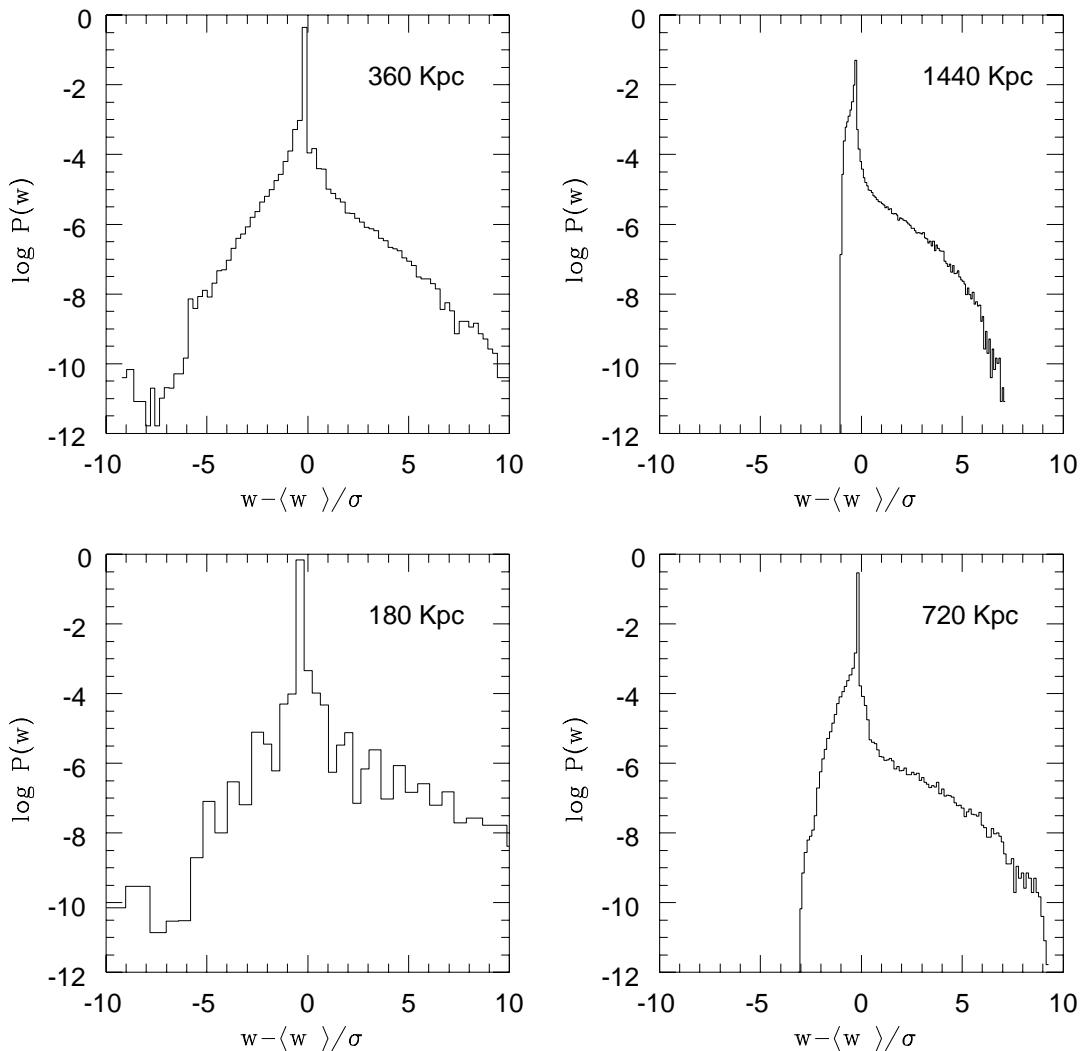

FIG. 4.—Same as Fig. 2, but for catalog C_{cen}

TABLE 4

RESULTS FOR C_{cen}

Scale (h^{-1} Mpc)	99.9%	3 σ	4 σ	5 σ	Voids
A. Number of Structures					
0.18	28	655	550	397	25
0.36	13	109	93	103	1
0.72	7	4	7	8	0
1.44	1	2	3	3	0
B. Morphology					
0.18	1.00	0.90	0.93	0.94	0.98
0.36	0.61	0.68	0.60	0.66	0.72
0.72	0.50	0.32	0.35	0.45	...
1.44	0.28	0.50	0.41	0.42	...

NOTE.—Same as Table 2, but for catalog C_{cen}.

6.2. Search for Segregation

Having identified the substructures, we tried to search for any evidence of segregation in luminosity and/or color. Recently, some evidence of morphological segregation within Coma has been found (Andreon 1996). Unfortunately, we did not have enough morphological information to attempt an analysis of morphological segregation among the substructures that we found. In Figure 5, we show that there is no evidence that the different subgroups observed within the central region of Coma differ as far as color distribution $b - r$ is concerned. One must, however, keep in mind that this color index is not strongly correlated with absolute b magnitude, so that from this figure one cannot draw any conclusion about the presence of morphological segregation. We will examine these and other aspects

of luminosity functions within Coma in a forthcoming paper.

7. STATISTICAL ROBUSTNESS AND PHYSICAL SIGNIFICANCE

Until now, we have not tried to draw from this wavelet analysis of the combined angular-redshift distribution any conclusion about the real phase- and configuration-space structure of Coma. Before performing this further step, one should verify that our catalog does not suffer from any systematic selection biases or from other types of systematic effects like those induced by redshift distortions, as described by Regős & Geller (1989) and Praton & Schneider (1994). About these latter we note that they have little significance for a cluster like Coma, because it lies at a distance of about 68 h^{-1} Mpc, and from Table 5 we note that the velocity dispersion of the structures found at a scale of 0.72 h^{-1} Mpc are at most on the order of 100 km s^{-1}, so the Hubble flow term is dominant over the peculiar velocity *within* these structures.

On one hand, one can reasonably argue that because the structures that we find are well within the nonlinear virialized region on these scales, we are probing a region of the phase space detached from the Hubble flow, where the linearity between redshift and distance is completely lost. On the other hand, one also expects that the phase-space distribution within the nonlinear region should be well enough mixed within each clump (if there are any) that the substructures detected will correspond to substructures in velocity space.

In order to check this latter hypothesis, following a suggestion of the anonymous referee, we have repeated the
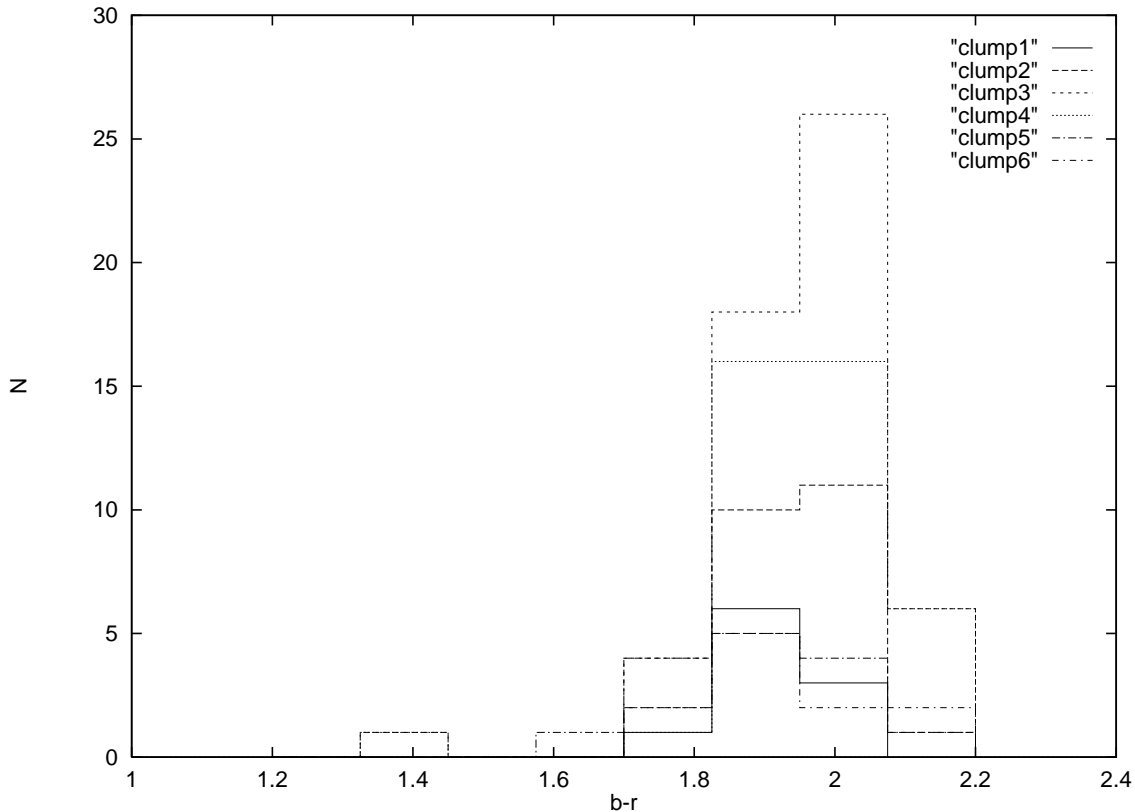

FIG. 5.—Color segregation. The different histograms refer to the substructures of Table 5 and are numbered according to the first column of that table.

TABLE 5

STRUCTURES DETECTED AT 720 h^{-1} kpc

Number of Clusters[a]	Number of Galaxies[b]	Dominant Galaxy (NGC)[c]	$(cz)_{min}$	$(cz)_{max}$	$\langle cz \rangle$	σ_{cz}	M_{vir}^{d}
1	18	4875	7756	7866	7805	30	6.9
2	34	4927	7510	7666	7594	39	16.8
3	71	4874 + 4839	6980	7350	7161	105	284
4	68	4864 + 4898	6572	6967	6775	102	286
5	22	4889	6356	6491	6421	34	10.2
6	19	4934 + 4840	6028	6164	6100	36	12.4

NOTE.—Redshifts are in km s^{-1}.

[a] Number associated with the clump.

[b] Number of galaxies inside the clump.

[c] Dominant galaxies of the clump.

[d] Estimated virialized mass in units of $10^{11} M_{\odot}$.

wavelet analysis on each of 20 realizations obtained by randomly "reshuffling" the original catalog, i.e., redistributing randomly the redshifts among the galaxies while keeping the angular coordinates fixed. The results are reported in Tables 6 and 7 and are consistent with those found by Escalera & Mazure (1992), who performed a similar analysis for two-dimensional catalogs. The average value of the number of structures is always smaller than that found in the original catalog, showing that the catalog itself is probably contaminated by some uncertainty, probably connected to the arbitrariness in the choice of the redshift limits, by some background contaminants, etc. However, note, for instance, that at the scale 0.44 h^{-1} Mpc the number of structures found is 54 in the main catalog, i.e., a value 3.13 σ larger than the mean yielded by reshuffling over the galaxies in Table 7. This corresponds to a confidence level of 99.82%, i.e., a 0.18% probability of false detection. On the scale 720 h^{-1} kpc, these figures become 99.33% for the confidence level and 0.67% for the probability of false detection. Interestingly enough, the mean value of structures found on this scale is 5, and a closer inspection

TABLE 6

STATISTICAL TESTS ON C_{cen}

Scale (h^{-1} kpc)	$\langle n \rangle$	σ_n	n_{min}	n_{max}
0.18	23.29	1.9	17	25
0.36	11.12	1.57	9	15
0.72	5.05	0.72	4	6
1.44	1.05	0.23	1	2

NOTES.—Statistics on a number of "reshufflings" of redshifts in catalog C_{cen}. The first column reports the scale, and the remaining columns give the average, standard deviation, and minimum and maximum numbers of structures found, respectively.

TABLE 7

STATISTICAL TESTS ON C

Scale (h^{-1} kpc)	$\langle n \rangle$	σ_n	n_{min}	n_{max}
0.47	42.12	3.79	33	48
0.94	17.47	3.47	12	22
1.88	2.29	0.57	1	3
3.76	1	0	1	1

NOTE.—Same as Table 6, but for catalog C.

reveals that the structures that do not disappear during the reshuffling are those numbered 2–5 in Table 5.

This test strengthens our confidence in the physical significance of most of the structures detected, particularly when filtering on the scale of 720 h^{-1} kpc. In this respect, our results are consistent with those found by Escalera & Mazure (1992) on two-dimensional maps of simulated clusters, which demonstrated the ability of the wavelet analysis to recover substructures that are traced even by few objects. We will perform a more quantitative analysis of the statistical significance of our wavelet analysis of combined angular-redshift catalogs in a forthcoming paper (Pagliaro et al. 1997a).

8. CONCLUSIONS AND DISCUSSION

During the last years, new redshift surveys and methods of analysis have allowed a more thorough understanding of the structure of the Coma Cluster (see, e.g., Mellier et al. 1988; Escalera, Slezak, & Mazure 1992; CD96; Biviano et al. 1996), with most of the effort going to ascertain whether it can be classified as relaxed and to unveil hidden substructures. While this cluster has often been modeled in the past under the assumptions of homogenous velocity structure and spherical symmetry (see, e.g., Kent & Gunn 1982), the most recent observational evidence points toward a more complex structure. The recent *ROSAT* images and two-dimensional optical analysis have strengthened the evidence for the existence of multiple substructure and suggest that Coma cannot be considered to be a relaxed cluster. In this respect, it is worth mentioning that in 1988 Mellier et al., by analyzing the isopleths within a two-dimensional map of the cluster, already had suggested the possible existence of nine density peaks. In this paper, we have investigated the nature of the Coma Cluster by performing a three-dimensional analysis of the combined angular-redshift distribution of the cluster. We have assembled a catalog of 798 galaxy redshifts, the largest presently available for the Coma Cluster. Then we developed a three-dimensional wavelet and segmentation structure analysis that has allowed us to find substructures on different scales and to describe them in a quantitative way. This powerful method of analysis has already provided excellent results in many fields of physics (see, e.g., Arneodo, Grasseau, & Holschneider 1988; Argoul et al. 1989; Slezak, Bijaoui, & Mars 1990; Fujiwara & Soda 1996; Grebenev et al. 1995).

Our results suggests that Coma cannot be considered a regular cluster of galaxies, but rather is filled with substructure on all scales ranging from 720 h^{-1} kpc to $\sim 4\ h^{-1}$ Mpc.

The general diminution of the mean morphological parameter, meaning more elongated shapes, and of the number of structures with the scale indicates a hierarchical distribution of the substructure.

We have examined the Coma Cluster using three different subsamples of our catalog (see Table 1), so we have insights within regions of different sizes with different resolutions. On a scale of about $2\ h^{-1}$ Mpc, our analysis of the extended Coma catalog suggests the presence of multiple substructure with spherical morphology (see Table 2). On this scale, a large number of voids are detected, and their shapes are rather spherical. In the same catalog, multiple substructure is still present at the scale $4\ h^{-1}$ Mpc: on this scale, shapes are more elongated ($\langle L \rangle = 0.67$). On scales 8 and $16\ h^{-1}$ Mpc, we find only two very elongated objects, in agreement with the histogram of Figure 1a. Voids on scales larger than $2\ h^{-1}$ Mpc are few and very elongated. Although we cannot draw any conclusion before having made a comparison with N-body simulations (Pagliaro et al. 1997b), the presence of hierarchically organized substructure seems to point to an evolutionary scenario in which the Coma Cluster and the galaxies included in the second peak of the histogram of the galaxy distribution in Figure 1a were not generated by the collapse of two large spherical density perturbations with different masses and radius of about $15\ h^{-1}$ Mpc, but by the merging of a large number of isolated spherical density perturbations of radii ranging from 1 to $3\ h^{-1}$ Mpc. This first rough picture of Coma's evolution becomes more evident if we examine catalogs C and C_{ext}.

Our analysis of the second catalog (C) suggests the presence of substructures on all the scales, with shapes becoming more elongated with increasing scale (see Table 3). Voids are detected only on scales 0.47–$0.94\ h^{-1}$ Mpc, and their shapes are rather spherical ($0.60 \leq \langle L \rangle \leq 0.94$).

On smaller scales (hundreds of kpc), we have concentrated our analysis on a central region with redshifts 5858 km s$^{-1} \leq cz \leq 8168$ km s^{-1}. This region includes the core of Coma, with the galaxies NGC 4874 ($\langle cz \rangle = 7131$ km s^{-1}) and NGC 4839 ($\langle cz \rangle = 7397$ km s^{-1}). Multiple substructures are found on scales 180–720 h^{-1} kpc, with rather spherical morphology ($0.50 \leq \langle L \rangle \leq 1.00$). A large number of spherical ($\langle L \rangle = 0.98$) voids is detected only on the smallest scale (180 h^{-1} kpc). We stress once again, however, the fact that the interpretation of substructures on such small scales in terms of *real* substructures in velocity (or position) space is not as strong, as noted in the previous paragraph.

Finally, we concentrate on the scale of 720 h^{-1} kpc, where we have detected seven substructures, which we show in Figure 6 and which coincide with the peaks that we find in the central region of the histogram of Figure 1b. To each of these objects we can associate a dominant galaxy. The mean redshifts of the objects are $cz \sim 5912$, 6100, 6421, 6775, 7161, 7594, and 7805 km s^{-1}. In Table 5, we report some statistics only for the clumps containing a significant number of objects. To each clump singled out, we can associate one or two dominant galaxies. These are (by
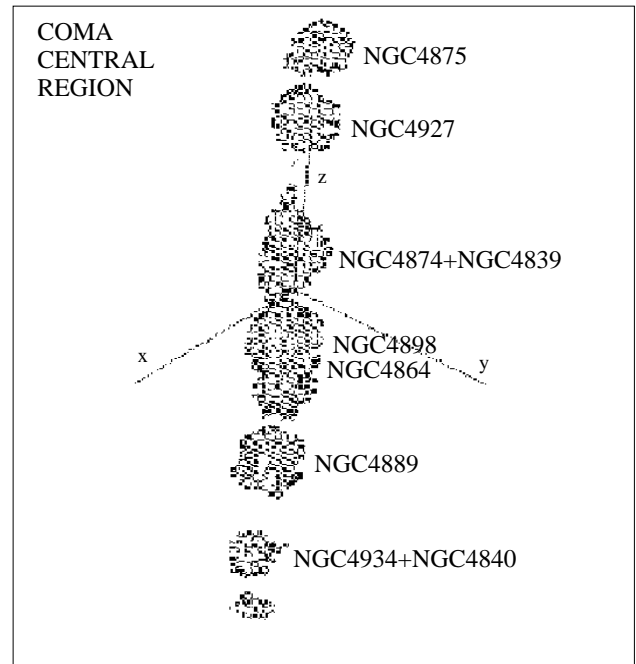

Fig. 6.—Substructures for the central region of Coma detected with a resolution of 720 h^{-1} kpc. The seven structures detected are clearly visible. Morphological parameter: $\langle L \rangle = 0.50$.

increasing redshift) NGC 4934 and 4840, NGC 4889, NGC 4898 and 4864, NGC 4874 and 4839, NGC 4927, and NGC 4875. We then confirm the presence of the two subclusters already described by CD96, but in addition we have found statistical evidence for the existence of more substructures in redshift space. All this evidence leads us to suggest that the Coma Cluster cannot be considered a regular cluster of galaxies and that its process of formation occurs through a *bottom-up* mechanism, as predicted by cold dark matter and mixed dark matter models.

We would finally like to stress the fact that from this analysis it is difficult to draw any conclusion about the evolutionary state of this cluster. Such an analysis would require some modeling of the evolutionary scenarios through comparison with high-resolution N-body simulations and a better understanding of the velocity field around Coma. We will report on these issues in a subsequent work (Pagliaro et al. 1997b).

REFERENCES

Abell, G. O. 1958, ApJS, 3, 211
Andreon, S. 1996, A&A, 314, 763
Argoul, F., Arneodo, A., Grasseau, G., Gagne, Y., Hopfinger, E. F., & Frisch, U. 1989, Nature, 338, 51
Arneodo, A., Grasseau, G., & Holschneider, M. 1988, Phys. Rev. Lett., 61, 2281
Baier, F. W., Fritze, K., & Tiersch, H. 1990, Astron. Nachr., 311, 89

Biviano, A., Durret, F., Gerbal, D., Le Fèvre, O., Lobo, C., Mazure, A., & Slezak, E. 1996, A&AS, 111, 265
Briel, U. G., Henry, J. P., & Böhringer, H. 1992, A&A, 259, L31
Colless, M., & Dunn, A. M. 1996, ApJ, 458, 435 (CD96)
Escalera, E., & Mazure, A. 1992, ApJ, 388, 23
Escalera, E., Slezak, E., & Mazure, A. 1992, A&A, 264, 379
Fitchett, M. J., & Webster, R. L. 1987, ApJ, 317, 653

Fujiwara, Y., & Soda, J. 1996, Prog. Theor. Phys., 95, 1059
Godwin, J., G., Metcalfe, N., & Peach, J. V. 1983, MNRAS, 202, 113
Grebenev, S. A., Forman, W., Jones, C., & Murray, S. 1995, ApJ, 445, 607
Grossmann, A., & Morlet, J. 1984, SIAM J. Math. Anal., 15, 723
———. 1987, in Mathematics and Physics: Lectures on Recent Results, Vol. 1, ed. L. Streit (Singapore: World Sci.), 135
Karachentsev, I. D., & Kopylov, A. I. 1990, MNRAS, 243, 390
Kent, S. M., & Gunn, J. E. 1982, AJ, 87, 945
Lega, E. 1994, Ph.D. thesis, Univ. Nice (L94)
Lega, E., Bijaoui, A., Alimi, J. M., & Scholl, H. 1996, A&A, 309, 23
Lega, E., Scholl, H., Alimi, J.-M., Bijaoui, A., & Bury, P. 1995, Parallel Comput., 21, 265
Mellier, Y., Mathez, G., Mazure, A., Chauvineau, B., & Proust, D. 1988, A&A, 199, 67

Pagliaro, A., Antonuccio-Delogu, V., Becciani, U., & Gambera, M. 1997a, in preparation
———. 1997b, in preparation
Pagliaro, A., & Becciani, U. 1997, in preparation
Praton, E. A., & Schneider, S. E. 1994, ApJ, 422, 46
Regős, E., & Geller, M. J. 1989, AJ, 98, 755
Rosenfeld, A. 1969, Picture Processing by Computer (New York: Academic)
Sarazin, C. L. 1986, in Radio Continuum Processes in Clusters of Galaxies, ed. C. P. O'Dea & J. M. Uson (Green Bank, WV: NRAO), 23
Slezak, E., Bijaoui, A., & Mars, G. 1990, A&A, 227, 301
White, S. D. M., Briel, U. G., & Henry, J. P. 1993, MNRAS, 261, L8
Zwicky, F. 1933, Helvetica Phys. Acta, 6, 10